



Stepwise tuning of the doping and thickness of a-Si:H(p) emitter layer to improve the performance of c-Si(n)/a-Si:H(p) heterojunction solar cells

Venkanna Kanneboina¹, Ramakrishna Madaka¹, and Pratima Agarwal^{1,2,*}

¹Department of Physics, Indian Institute of Technology Guwahati, Guwahati, Assam 781039, India

²Centre for Energy, Indian Institute of Technology Guwahati, Guwahati, Assam 781039, India

Received: 23 November 2020

Accepted: 23 December 2020

© The Author(s), under exclusive licence to Springer Science+Business Media, LLC part of Springer Nature 2021

ABSTRACT

Crystalline silicon (c-Si)/ hydrogenated amorphous silicon (a-Si:H) heterojunction (Ag/Al/c-Si(n)/a-Si:H(i)/a-Si:H(p)/ITO/Ag) solar cells were fabricated by RF-PECVD technique. The efficiency (η), short circuit current density (J_{sc}) and fill factor (FF) of the heterojunction (HJ) solar cells were improved from 10 to 17%, 24 to 32 mA/cm² and 0.60 to 0.74 respectively through systematic tuning of processing steps; the thickness and doping of a-Si:H(p) layer respectively. High open circuit voltage (V_{oc}) of 705 mV could be achieved by improving the interfaces between the a-Si:H layers and c-Si by inserting an ultrathin intrinsic a-Si:H film using H₂ plasma treatment on c-Si(n) wafer and a-Si:H(i) layer respectively. Simultaneously, other solar parameters like J_{sc} and FF were also improved step by step by carefully adjusting the gas flow rate and deposition time of doped a-Si:H(p) layer. By increasing the doping of a-Si:H(p) layer, electric field at the interface could be enhanced, which led to the immediate separation of electron–hole pair and thus improving the solar cell parameters. This is also confirmed by external quantum efficiency (EQE) spectra measured with and without external reverse bias.

1 Introduction

The quality of doped a-Si:H layer is very crucial to improve the performance of c-Si/a-Si:H heterojunction (HJ) solar cells, which have demonstrated very promising performance [1–4]. In these heterojunction solar cells, the p – n junction is made between the c-Si wafer and thin a-Si:H layer, which is either p -type or n -type doped depending upon if the c-Si is n or p

type. The photons are absorbed mainly in c-Si wafer, whereas the role of doped a-Si:H layer is to provide electric field at the junction to separate the photogenerated electron–hole pairs. The opto-electronic properties of a-Si:H(p) thin films are affected significantly by deposition conditions like substrate temperature, process pressure, hydrogen and silane gas flow rate, hydrogen dilution etc. Though extensive research has been carried out to study the influence of deposition

Address correspondence to E-mail: pratima@iitg.ac.in

parameters on the properties of a-Si:H(*i*) thin films [5–8], however, very few research groups have focused their attention on a-Si:H(*p*) films [9–12].

The a-Si:H, hydrogenated poly/nano/micro-crystallite silicon, hydrogenated silicon carbide (a-SiC:H) thin films have been used as emitter layer in c-Si based solar cells to increase its band gap, which further reduces the parasitic absorption and improves short wavelength response of the solar cells [5, 11, 12]. The wider bandgap of *p*-layer creates band discontinuity at *i/p* interface resulting in recombination losses at *i/p* interface which deteriorate the solar cell performance. So, appropriate bandgap matching between *p* and *i*-layers is necessary to reduce carrier recombination losses at the *i/p* interface. However, deposition of nc-Si:H require high temperature and power density, which may severely damage the microstructure of the a-Si:H(*i*) passivation layer hence reduce the V_{oc} of the silicon heterojunction (SHJ) solar cells. The quality of *p*-emitter layer is directly related to the efficiency of n-type SHJ solar cells. The *p*-emitter layer requires sufficiently high doping to form required internal electric field and also good interface properties between *i/p*-layers and *p*/indium tin oxide (ITO) layers [13, 14].

SHJ solar cells are characterized by the relatively higher open circuit voltage as compared to conventional c-Si solar cells. The open circuit voltage in these cells depends upon the quality of interface between the c-Si and a-Si:H. High open circuit voltage of SHJ solar cells was obtained mainly by superior passivation quality of wafer and ultra thin a-Si:H(*i*) layer to suppress the recombination of charge carriers by reducing the defect density, voids and strengthening the hydrogen bonding at the c-Si and *i*-layer interfaces and also *i/p* interfaces. This could be achieved by exposing the surfaces of c-Si and a-Si:H(*i*) layers to hydrogen plasma during fabrication of solar cells [15, 16].

Most of the research groups are focused on double side SHJ solar cells to improve the performance of the devices and less attention is paid to the single side solar cells [14, 17–23]. The fabrication of double side silicon junction solar cells requires additional steps of depositing the intrinsic and doped a-Si:H to act as passivation layer and improved back surface field. Current reported highest efficiency is 26.6% on *n* and 26.1% on *p*-type c-Si wafer with interdigitated back contact silicon heterojunction (IBC-SHJ) (double side) solar cell technology [24–26]. However, it is very

challenging to fabricate and achieve such high performance solar cells due to lack of quality Si wafers and sophisticated techniques and many complicated process steps and contamination problems. Whereas, for fabrication of single side solar cells, only electrode has to be deposited on the back surface of the Si wafer, thus the processing is simpler, less time consuming and reduces the cost as well. The only challenge is optimizing the thickness and quality of intrinsic and doped a-Si:H to improve the quality of interfaces. In our earlier paper, we have reported high V_{oc} of 711 mV for one side c-Si (*n*)/a-Si:H (*p*) HJ solar cells [27]. This V_{oc} is almost comparable with double-side SHJ solar cells. These results suggested that single side c-Si/a-Si:H heterojunction solar cells are capable of high open circuit voltage and efficiency. Those results have encouraged us to further improve efficiency of one side c-Si/a-Si:H HJ solar cells through optimization of *i*- and *p*-layers. Figure 1 shows the schematic band bending diagram of our fabricated single side c-Si(*n*)/a-Si:H(*p*) heterojunction solar cells.

This paper presents influence of boron doping concentration of a-Si:H(*p*) layer and thickness of intrinsic as well as p-type a-Si:H layers on the performance of c-Si/a-Si:H single side HJ solar cells. Our main motivation behind this work has been to further improve the efficiency of single side HJ solar cells by optimizing the thickness and doping of intrinsic and boron doped a-Si:H layers without compromising on the open circuit voltage. By increasing the doping of *p*-layer and decreasing the thickness of both intrinsic and doped a-Si:H layers, we could achieve the efficiency of > 17% with a high V_{oc} of 705 mV. The efficiency of our cells is comparable, whereas the open circuit voltage value is higher than that reported by other research groups for single side SHJ.

The paper presents the systematic investigation that has been carried out to study the influence of diborane flow rate and thickness of intrinsic and doped a-Si:H layers to identify their role on the performance of c-Si/a-Si:H HJ solar cells. The EQE measurements confirm that electric field at the interfaces is significantly improved when doping of the *p*-layer is higher and thickness is low.

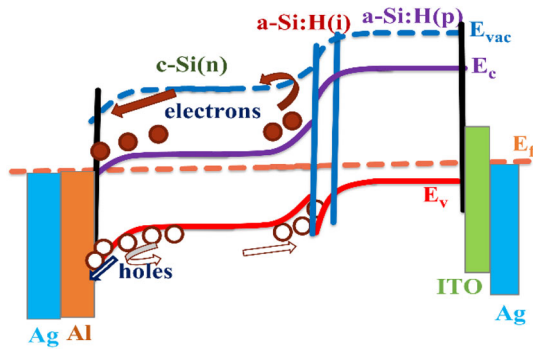


Fig. 1 Schematic band bending diagram of single side c-Si(n)/a-Si:H(p) heterojunction solar cells

2 Experimental details

2.1 Fabrication of c-Si/a-Si:H heterojunction solar cells

One side Ag/Al/c-Si(n)/a-Si:H(i)/a-Si:H(p)/ITO/Ag HJ solar cells were fabricated by rf plasma CVD in multi-chamber system. Schematic band bending diagram of fabricated c-Si(n)/a-Si:H(p) heterojunction solar cells is shown in Fig. 1. Standard RCA cleaning process is used for cleaning the Si wafers [28, 29]. The details of other process on c-Si prior to the fabrication of single side HJ solar cells (Al deposition, annealing at 400 °C and H₂ plasma treatment (HPT) for 10 min of c-Si wafer) are presented in our previous paper [27]. Subsequently, thin (35–33 nm) *i*-layer was deposited on this plasma treated c-Si surface. The silicon wafer was then moved to *p*-layer deposition chamber, where the *i*-layer was exposed to 2 min HPT prior to the *p*-layer deposition. Thin a-Si:H(*p*) film with thickness as low as ~ 10 or 7 nm with different boron doping concentration was deposited for completing the solar cells. Table 1 summarizes the deposition parameters used for fabrication of one side c-Si/a-Si:H HJ solar cells.

During H₂ plasma treatment, 50 SCCM (standard cubic centimetre per minute) flow rate of pure hydrogen was used and other deposition conditions were kept same as those for *i*-layer. We have adopted similar procedure for deposition of ITO layer and Ag contacts as presented in our previous paper [27]. The doping of the *p*-layer was changed by changing the B₂H₆ flow rate during deposition and performance of the cells was used as feedback to optimize the thickness of a-Si:H layers to improve the efficiency of the cells.

The *I*–*V* characteristics measurements on c-Si/a-Si:H HJ solar cells were done using Xenon lamp with AM1.5 conditions (power density 100 mW/cm²). External Quantum Efficiency (EQE) measurements were carried out in the wavelength range of 350–1100 nm. Calibrated Si photo diode was used as reference for calculating the EQE of the solar cells [5, 27, 30].

3 Results and discussion

3.1 Influence of doping and thickness of a-Si:H(*p*) layer on c-Si/a-Si:H solar cells

3.1.1 Current voltage measurement of solar cells

The dark current density (*J*)–voltage (*V*) characteristics of all the c-Si/a-Si:H HJ solar cells under reverse and forward bias conditions are shown in Fig. 2. A systematic decrease in reverse saturation current density (*J*₀) of all cells is observed from *nip5* to *nip10*; as the diborane flow rate is increased and/or thickness of the *i*- and *p*-layer is decreased. The lowest value of *J*₀ is obtained for the *nip10* cell, which was fabricated with diborane flow rate at 20 SCCM and *i*- and *p*-layers being 5 nm and 7 nm thick, respectively. For all the cells, the high injection region started at a forward bias of about 700 mV. This is an indication that the solar cells are likely to have a high *V*_{oc} of ~ 700 mV. The decrease in magnitude of reverse saturation current with increase in the doping of the *p*-layer and reduction in thickness of a-Si:H layers also suggests an increase in efficiency.

Figure 3 shows the current density–voltage (*J*–*V*) curve of c-Si/a-Si:H solar cells for AM1.5 illuminations. The *J*–*V* characteristics in dark of two cells (*nip5* and *nip10*) has also been included in Fig. 3 for comparison. The values of solar cell parameter; *J*_{sc}, *V*_{oc}, *FF* and *η* for all the cells calculated from the *J*–*V* curve are given in Table 2. These values are systematically increased from *nip5* to *nip10* cells. A crossover of *J*–*V* characteristics in dark and under illuminations is observed around 700 mV for the *nip5*–*nip10* cells. The open circuit voltage has systematically increased from 694 to 705 mV for *nip5* to *nip10* cells respectively. These values are slightly lower than reported value of 711 mV in previous paper [27], however, still the present *V*_{oc} values are higher than values reported by other groups so far for single sided HJ solar

Table 1 Deposition conditions for c-Si/a-Si:H HJ solar cells

Cell	Layer	H ₂ (SCCM)	SiH ₄ (SCCM)	B ₂ H ₆ (SCCM)	PP (mbar)	Dep. temp. (°C)	Layer thickness (nm)
nip5	a-Si:H(p)	60	4	6	0.42	200	10
	a-Si:H(i)	50	–	–			7
nip6	a-Si:H(p)	60	–	10	–	–	10
	a-Si:H(i)	50	–	–			7
nip7	a-Si:H(p)	60	–	14	–	–	10
	a-Si:H(i)	50	–	–			7
nip8	a-Si:H(p)	60	–	14	–	–	10
	a-Si:H(i)	50	–	–			5
nip9	a-Si:H(p)	60	–	20	–	–	10
	a-Si:H(i)	50	–	–			5
nip10	a-Si:H(p)	60	–	20	–	–	7
	a-Si:H(i)	50	–	–			5

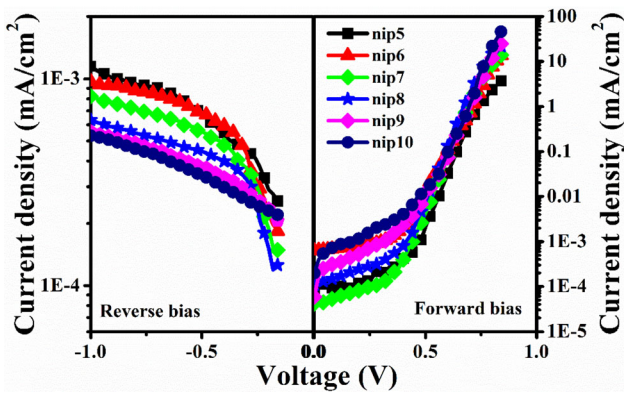


Fig. 2 Dark J - V characteristics of cells under reverse and forward bias condition

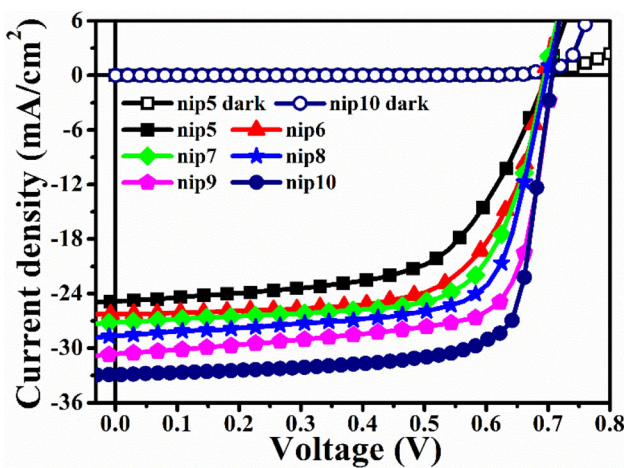


Fig. 3 J - V characteristics of Ag/Al/c-Si(n)/a-Si:H(i)/a-Si:H(p)/ITO/Ag HJ solar cells

cells on n - and p -type c-Si [18–23]. By optimizing the doping of p -layer and thickness of a-Si:H layers, we have achieved high V_{oc} of 705 mV and efficiency of 17.3% for single sided c-Si/a-Si:H HJ solar cells fabricated at diborane flow rate at 20 SCCM and i - and p -layers being 5 nm and 7 nm thick respectively. This significant improvement in J_{sc} and V_{oc} parameters is due to the systematic increase of doping of p - and decrease of thickness of i - and p -layer accompanied with the decrement of void fraction at n/i and i/p interfaces along with the overall improvement in microstructure of a-Si:H layers as discussed in the subsequent sections.

The detailed studies of influence of HPT on c-Si(n) and a-Si:H(i) layer were presented in previous paper [27]. These results suggested that HPT has passivated c-Si surface, i -layer, interfaces and also improve the microstructure of a-Si:H layers of c-Si/a-Si:H HJ solar cells. Therefore, $nip5$ – $nip10$ solar cells have good interface and carrier transport properties by reduction of recombination losses of photo generated carriers [16]. In this series of cells, the V_{oc} has increased with increase in boron doping of p -layer and we have obtained high V_{oc} of 705 mV for $nip9$ and $nip10$ cells. The reason for systematic increase in current density and efficiency of the solar cells is discussed below.

In case of p - n junction, the depletion region width and effective electric field depends upon the doping concentration on both sides. Generally, one side of the junction is lightly doped, which is used as absorber layer in these devices. The effective electric field, which is given by the ionized donor/acceptor

Table 2 The solar cell parameters of c-Si/a-Si:H HJ solar cells

Cell	J-V measurement								EQE measurement	
	J_{sc} (mA/cm ²)	V_{oc} (mV)	J_{max} (mA/cm ²)	V_{max} (mV)	FF	η (%)	R_{sh} (Ω cm ²)	R_s (Ω cm ²)	J_{sc} (mA/cm ²)	η (%)
<i>nip5</i>	24.81	694	20.10	519	0.60	10.43	185	7.6	23.47	9.87
<i>nip6</i>	26.23	694	22.85	533	0.67	12.18	323	4.3	24.92	11.60
<i>nip7</i>	27.15	695	23.06	563	0.69	12.98	307	3.8	26.33	12.61
<i>nip8</i>	28.65	698	24.03	483	0.70	14.01	305	3.0	28.20	13.79
<i>nip9</i>	31.07	705	26.83	602	0.74	16.15	315	2.5	30.69	15.96
<i>nip10</i>	32.72	705	28.11	620	0.75	17.30	583	2.0	32.11	16.97

concentration in the depletion region, also depends upon the total charge in the depletion region, in other words, on the thickness of the depletion region as well. If the thickness of the heavily doped region is less than the depletion region width given by the charge neutrality condition, the effective electric field is reduced, which is detrimental in separating the photo generated electron–hole pairs. Thus, it is necessary to have sufficient thickness of heavily doped region to support the electric field. However, as the thickness of this region is increased, more photons are absorbed here, which do not contribute to the short circuit current of the solar cells. It is therefore necessary to further increase the doping of this region such that the thickness is equal to the necessary depletion width and maintain the high electric field at the junction. Also, it should not be more than the depletion width so as to prevent the photon absorption in the neutral region near the surface of solar cells. In case of a-Si:H, the defect states at the interface also cause a distortion of electric field in the depletion region and influence the charge transport. The thickness of intrinsic a-Si:H layer is also to be optimized to minimize the series resistance of the device while maintain the electric field at the interface.

Now, let us discuss our results; an increase in doping of *p*-layer, as a result of increase in diborane flow rate, provided enough charge density in the depletion region to overcome any electric field reduction/distortion at the interface. An increase in electric field at the interface also helps in quick separation of photo-generated charge carriers before these recombine, which further increased the J_{sc} . Role and importance of number of layers such as doped, intrinsic, ITO layers and metal contacts in the improvement of the performance of the solar cells

and their band bending is clearly shown schematically in Fig. 1 for better understanding of the devices. In case of cells (*nip5*) prepared at low boron concentration (DBFR 6 SCCM), the J_{sc} of 24.81 mA/cm² was obtained, which was enhanced to 26.23 and 27.15 mA/cm² for *nip6* (DBFR 10 SCCM) and *nip7* (DBFR 14 SCCM) cells, respectively, along with a systematic increase in *FF*. To further improve J_{sc} , thickness of *i*-layer was decreased to 5 nm from 7 nm for *nip8* keeping the DBFR at 14 SCCM. The J_{sc} of *nip8* has further improved to 28.65 mA/cm² due to low absorption of photons in the less thick *i*-layer than *nip7* and also photo generated carriers have smaller path length to reach contacts [18, 31]. This J_{sc} value (28.65 mA/cm²) is still lower than that expected in SHJ solar cells. In an attempt to increase the J_{sc} further, DBFR was again increased to 20 SCCM to increase the doping of *p*-layer. This increase in doping resulted in the decrease of series resistance of the cell; J_{sc} value was increased to 31.07 mA/cm² for *nip9* cell along with the V_{oc} of 705 mV and *FF* of 0.74. To further increase the J_{sc} , another solar cell (*nip10*) was fabricated with a lower thickness (7 nm) of *p*-layer keeping DBFR at 20 SCCM and thickness of *i*-layer at 5 nm. The J_{sc} for this cell (*nip10*) was 32.72 mA/cm² with a V_{oc} of 705 mV and *FF* of 0.75. This increment in J_{sc} is mainly due to improvement in the generation and collection of free charge carriers, reducing the resistance losses and decreasing the minority carrier path length by decreasing the thickness of *i*- and *p*-layers. We could have obtained best *FF* values for *nip9* and *nip10* cells are 0.74 and 0.75 respectively. The *FF* is mainly depend on series resistance as well as shunt resistance and fraction of voids in the different layers [32–34]. The values of shunt (R_{sh}) and series (R_s) resistance are calculated from the *J*–*V* curve of the solar cells and listed in Table 2. As

evident from this Table 2, there is a systematic decrease in series resistance and increase in shunt resistance as the DBFR is increased and thickness of *i*- and *p*-layer is reduced from *nip5* to *nip10* cells. The improvement in V_{oc} , J_{sc} and FF resulted in improvement in the efficiency of solar cells. We have achieved best efficiency of 17.3% for *nip10* cell.

3.1.2 Quantum efficiency measurement of solar cells

The external quantum efficiency (EQE) spectra of c-Si/a-Si:H heterojunction *nip5*–*nip10* solar cells shown in Fig. 4. The highest quantum efficiency of *nip10* cells is nearly 94 to 96% over a broad spectral range (450–850 nm). For *nip5* cell EQE is $\sim 77\%$ in the spectral range of 550–800 nm. The EQE has slightly enhanced for *nip6* cell as compared to *nip5* cell. For *nip7* cell, EQE has further improved in lower (450–550 nm) and mid (550–800 nm) wavelength range. This is due to better collection of charge carriers and smaller series resistance with increase in doping of *p*-layer. A significant improvement in EQE ($\sim 87\%$), over a broad spectral range (500–850 nm), for *nip8* is observed. The cell was fabricated with the same DBFR (14 SCCM) as that for *nip7*, but with a lower thickness of *i*-layer. For this cell, the EQE is more than 70%, both in the low wavelength region ~ 450 nm as well as high wavelength region ~ 900 nm. For *nip9* and *nip10*, where the doping of *p*-layer was increased along with a change in thickness of *p*-layer keeping the thickness of the *i*-layer same as that for *nip8*, EQE crossed 90% in the mid wavelength range along with a significant improvement in both low and high wavelength

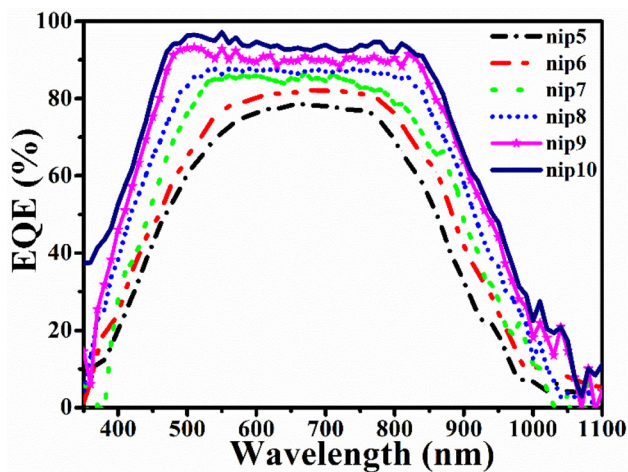


Fig. 4 EQE spectra of c-Si/a-Si:H HJ solar cells

range. The EQE for these cells is $\sim 80\%$ at 450 nm as well as 850 nm. The improvement at low wavelength region is mainly due to decrement of thickness of *p*- and *i*-layer, which helped more photons to be absorbed in the c-Si wafer. A significant improvement in EQE in both low and high wavelength range is a mark of good quality abrupt junctions [35]. The EQE spectra are used to estimate the integrated J_{sc} for AM1.5G spectra and the values are listed in Table 2. It is evident that J_{sc} values obtained from I - V measurements and calculated from EQE spectra are in good agreement. Table 2 also lists the efficiency of these solar cells calculated using the J_{sc} values from EQE spectra and V_{oc} and FF obtained from I - V measurement.

To check if the improvement in EQE is due to only less absorption of photons in *p* and *i*-layer, or whether the increase in doping concentration had any role in improving the electric field at the *p*/*i* and *i*/*n* interfaces, the EQE spectra are measured under slight reverse bias condition (-1 V). Figure 5 show EQE spectra under no bias as well as under reverse bias conditions for each of the cell fabricated for this study. It can be seen from these spectra that for *nip5* to *nip8* cells, the EQE measured under reverse bias conditions is more than that under no bias condition. This clearly indicates that with increase in doping of *p*-layer, though, we have been able to collect more carriers to the respective electrodes, the electric field at the interface and in the *i*-layer is still not sufficient to sweep all the carriers to the respective electrodes. By decreasing the thickness of *i*-layer in *nip8* cell, response in the mid wavelength range, as well as in the low and high wavelength range was significantly improved as compared to *nip7* cell, which has the same doping and thickness of *p*-layer. This is due to less number of photons are absorbed in the *i*-layer. When the doping of *p*-layer is further increased for *nip9*, not only EQE has increased, the response under zero bias condition and reverse bias condition has also been almost same. For *nip10* cell, for which the thickness of *p*-layer was decreased to 7 nm, the EQE is almost ~ 94 – 96% in a broad wavelength range with an increase in response below 400 nm and no change in EQE under reverse bias conditions. The increase in response below 400 nm for *nip10* cell is attributed to the less absorption in *p*-layer. The observations also suggest that the *p*-layer deposited with a DBFR of 20 SCCM provides enough electric field at the interface to sweep all the photo-generated

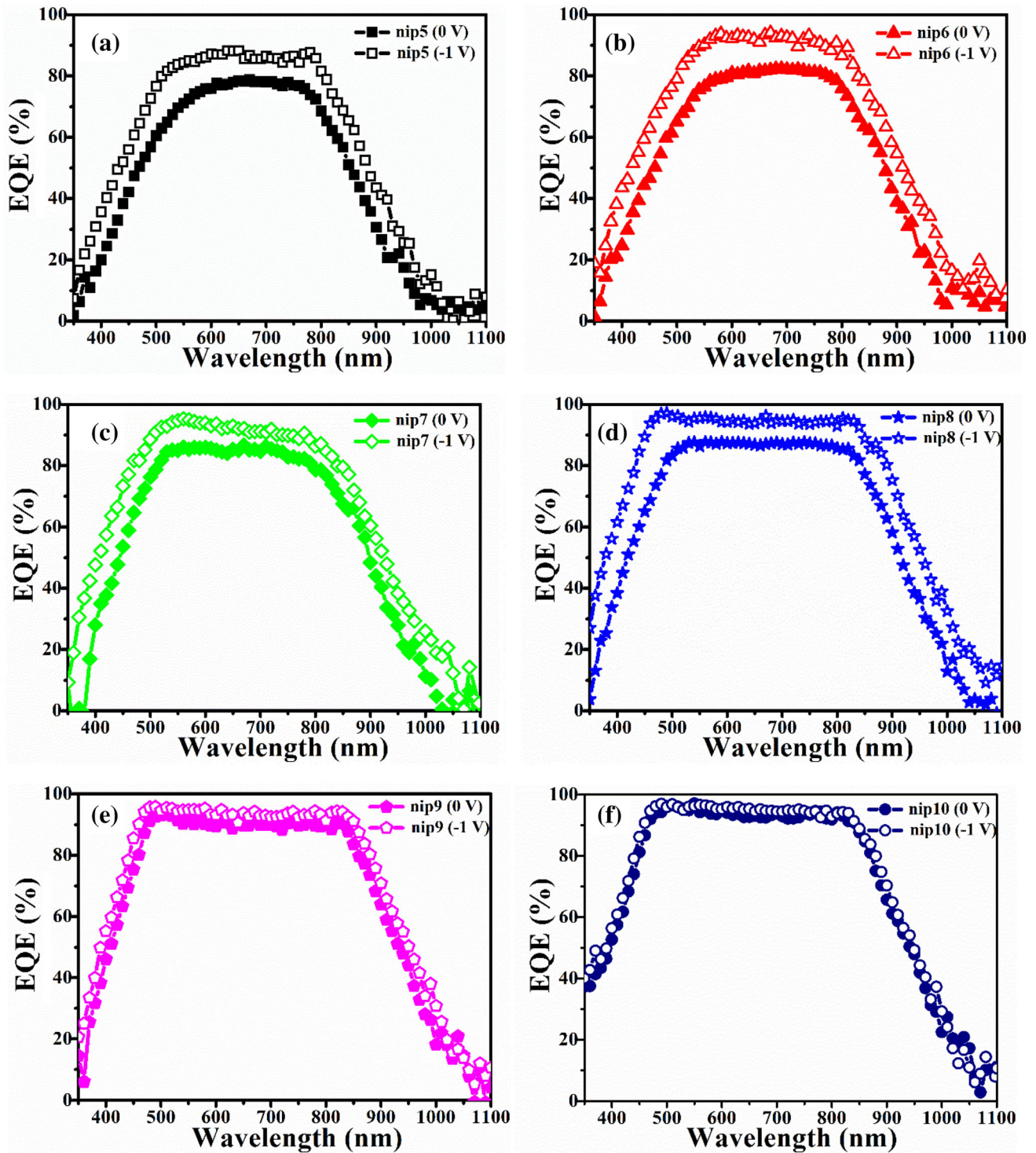


Fig. 5 a–f EQE spectra of c-Si/a-Si:H solar cells with and without reverse biasing

charge carriers to the respective electrodes and reduces recombination loss at bulk of layer and the *i/p* as well as *p*/ITO interfaces.

4 Conclusion

One side c-Si/a-Si:H heterojunction solar cells were fabricated by varying doping and thickness of a-Si:H(*p*) layer. We have achieved high open circuit

voltage of 705 mV and efficiency of 17.3% on *n*-type c-Si wafers. The efficiency, FF and J_{sc} have enhanced from 10 to 17%, 0.60 to 0.74 and 24 to 32 mA/cm² respectively. These high performance device results are obtained mainly due to HPT on c-Si and a-Si:H(*i*) layer, increase of doping and decrease of thickness of a-Si:H(*p*) layer. Electric field at the junction of solar cells has enhanced significantly with increase in doping of *p*-layer. Generated electron–hole pairs are separated immediately and swept to metal contacts without any recombination losses at the interfaces and bulk of a-Si:H layers by enhanced electric field. Further, this is confirmed by EQE measurements with and without external biasing conditions.

Acknowledgment

Grant received from Department of Science and Technology (DST) (Grant No. DST/TM/SERI/2K11/78(G)), India and Defence Research and Development Organization (DRDO) (Grant No. ERIP/ER/0900376/M/01/1297), India for establishing the Multi-chamber RFPECVD system.

Data availability

The raw/processed data required to reproduce these findings cannot be shared at this time as the data also forms part of an ongoing study.

Compliance with ethical standards

Conflict of interest The authors declare that they have no conflict of interest.

References

1. K. Masuko, M. Shigematsu, T. Hashiguchi, D. Fujishima, M. Kai, N. Yoshimura, T. Yamaguchi, Y. Ichihashi, T. Mishima, N. Matsubara, T. Yamanishi, T. Takahama, M. Taguchi, E. Maruyama, S. Okamoto, *IEEE J. Photovolt.* **4**, 1433 (2014)
2. M. Taguchi, A. Yano, S. Tohoda, K. Matsuyama, Y. Nakamura, T. Nishiwaki, K. Fujita, E. Maruyama, *IEEE J. Photovolt.* **4**, 96 (2014)
3. Y. Tsunomura, Y. Yoshimine, M. Taguchi, T. Baba, T. Kinoshita, H. Kanno, H. Sakata, E. Maruyama, M. Tanaka, *Sol. Energy Mater. Sol. Cells* **93**, 670 (2009)
4. M.A. Green, Y. Hishikawa, A.W.Y.H. Baillie, E.D. Dunlop, D.H. Levi, *Prog. Photovolt. Res. Appl.* **26**, 3 (2018)
5. R. Madaka, V. Kanneboina, P. Agarwal, *Semicond. Sci. Technol.* **33**, 3 (2018)
6. P. Gogoi, P. Agarwal, *Sol. Energy Mater. Sol. Cells* **93**, 199 (2009)
7. U. Kroll, J. Meier, A. Shah, S. Mikhailov, J. Weber, *J. Appl. Phys.* **80**, 4971 (1996)
8. L. Hamui, B.M. Monroy, K.H. Kimb, A. López-Suárez, J. Santoyo-Salazar, M. López-López, P.R. Cabarrocas, G. Santana, *Mater. Sci. Semicond. Process.* **41**, 390 (2016)
9. C. Song, X. Wang, R. Huang, J. Song, Y. Guo, *Mater. Chem. Phys.* **142**, 292 (2013)
10. J.M. Westra, R.A.C.M.M. Van Swaaij, P. Šutta, K. Sharma, M. Creatore, M. Zeman, *Thin Solid Films* **568**, 38 (2014)
11. G. Hou, J. Fang, Q. Hua, C. Wei, J. Ni, *Sol. Energy Mater. Sol. Cells* **134**, 395 (2015)
12. F. Wang, X. Zhang, L. Wang, J. Fang, C. Wei, *Sol. Energy* **108**, 308 (2014)
13. J. Ramanujam, A. Verma, *Mater. Express* **2**, 177 (2012)
14. S. De Wolf, A. Descoedres, Z.C. Holman, C. Ballif, *Green* **2**, 7 (2012)
15. A. Matsuda, *J. Non. Cryst. Solids* **338–340**, 1 (2004)
16. F. Meng, L. Shen, J. Shi, L. Zhang, J. Liu, Y. Liu, Z. Liu, *Appl. Phys. Lett.* **107**, 223901 (2015)
17. M.F. Abdullah, A.M. Hasim, *J. Mater. Sci.* **54**, 911 (2019)
18. H. Fujiwara, M. Kondo, *J. Appl. Phys.* **101**, 054516 (2007)
19. H. Fujiwara, M. Kondo, *Appl. Phys. Lett.* **90**, 2005 (2007)
20. H. Fujiwara, T. Kaneko, M. Kondo, *Sol. Energy Mater. Sol. Cells* **93**, 725 (2009)
21. W.K. Oh, S.Q. Hussain, Y.J. Lee, Y. Lee, S. Ahn, J. Yi, *Mater. Res. Bull.* **47**, 3032 (2012)
22. T. H. Wang, M. R. Page, E. Iwaniczko, Q. Wang, Y. Xu, Y. Yan, L. Roybal, D. Levi, R. Bauer, and H. M. Branz, in *NREL/CP-520-38942* (2005), pp. 1–5.
23. T. H. Wang, E. Iwaniczko, M. R. Page, Q. Wang, Y. Xu, Y. Yan, D. Levi, L. Roybal, R. Bauer, and H. M. Branz, in *IEEE 4th World Conf.* (2006), pp. 1439–1442.
24. K. Yoshikawa, W. Yoshida, T. Irie, H. Kawasaki, K. Konishi, H. Ishibashi, T. Asatani, D. Adachi, M. Kanematsu, H. Uzu, K. Yamamoto, *Sol. Energy Mater. Sol. Cells* **173**, 37 (2017)
25. K. Yoshikawa, H. Kawasaki, W. Yoshida, T. Irie, K. Konishi, K. Nakano, T. Uto, D. Adachi, M. Kanematsu, H. Uzu, K. Yamamoto, *Nat. Energy* **2**, 17032 (2017)
26. F. Haase, C. Hollemann, S. Schäfer, A. Merkle, M. Rienäcker, J. Krügener, R. Brendel, R. Peibst, *Sol. Energy Mater. Sol. Cells* **186**, 184 (2018)
27. V. Kanneboina, R. Madaka, P. Agarwal, *Sol. Energy* **166**, 255 (2018)
28. W. Kern, Puotinen D A. *RCA Rev.* **31**, 187 (1970)

29. W. Kern, *J. Electrochem. Soc.* **137**, 1887 (1990)
30. R. Madaka, V. Kanneboina, P. Agarwal, *J. Electron. Mater.* **47**, 4710 (2018)
31. M.R. Page, E. Iwaniczko, Y.Q. Xu, L. Roybal, F. Hasoon, Q. Wang, R.S. Crandall, *Thin Solid Films* **519**, 4527 (2011)
32. H. Sonobe, A. Sato, S. Shimizu, T. Matsui, M. Kondo, A. Matsuda, *Thin Solid Films* **502**, 306 (2006)
33. Q. Wang, *Sol. Energy Mater. Sol. Cells* **129**, 64 (2014)
34. S.Y. Lee, J.H. Shim, D.J. You, S.W. Ahn, H.M. Lee, *Sol. Energy Mater. Sol. Cells* **95**, 142 (2011)
35. M. Agarwal, A. Pawar, N. Wadibhasme, R. Dusane, *Sol. Energy* **144**, 417 (2017)

Publisher's Note Springer Nature remains neutral with regard to jurisdictional claims in published maps and institutional affiliations.

Terms and Conditions

Springer Nature journal content, brought to you courtesy of Springer Nature Customer Service Center GmbH (“Springer Nature”).

Springer Nature supports a reasonable amount of sharing of research papers by authors, subscribers and authorised users (“Users”), for small-scale personal, non-commercial use provided that all copyright, trade and service marks and other proprietary notices are maintained. By accessing, sharing, receiving or otherwise using the Springer Nature journal content you agree to these terms of use (“Terms”). For these purposes, Springer Nature considers academic use (by researchers and students) to be non-commercial.

These Terms are supplementary and will apply in addition to any applicable website terms and conditions, a relevant site licence or a personal subscription. These Terms will prevail over any conflict or ambiguity with regards to the relevant terms, a site licence or a personal subscription (to the extent of the conflict or ambiguity only). For Creative Commons-licensed articles, the terms of the Creative Commons license used will apply.

We collect and use personal data to provide access to the Springer Nature journal content. We may also use these personal data internally within ResearchGate and Springer Nature and as agreed share it, in an anonymised way, for purposes of tracking, analysis and reporting. We will not otherwise disclose your personal data outside the ResearchGate or the Springer Nature group of companies unless we have your permission as detailed in the Privacy Policy.

While Users may use the Springer Nature journal content for small scale, personal non-commercial use, it is important to note that Users may not:

1. use such content for the purpose of providing other users with access on a regular or large scale basis or as a means to circumvent access control;
2. use such content where to do so would be considered a criminal or statutory offence in any jurisdiction, or gives rise to civil liability, or is otherwise unlawful;
3. falsely or misleadingly imply or suggest endorsement, approval, sponsorship, or association unless explicitly agreed to by Springer Nature in writing;
4. use bots or other automated methods to access the content or redirect messages
5. override any security feature or exclusionary protocol; or
6. share the content in order to create substitute for Springer Nature products or services or a systematic database of Springer Nature journal content.

In line with the restriction against commercial use, Springer Nature does not permit the creation of a product or service that creates revenue, royalties, rent or income from our content or its inclusion as part of a paid for service or for other commercial gain. Springer Nature journal content cannot be used for inter-library loans and librarians may not upload Springer Nature journal content on a large scale into their, or any other, institutional repository.

These terms of use are reviewed regularly and may be amended at any time. Springer Nature is not obligated to publish any information or content on this website and may remove it or features or functionality at our sole discretion, at any time with or without notice. Springer Nature may revoke this licence to you at any time and remove access to any copies of the Springer Nature journal content which have been saved.

To the fullest extent permitted by law, Springer Nature makes no warranties, representations or guarantees to Users, either express or implied with respect to the Springer nature journal content and all parties disclaim and waive any implied warranties or warranties imposed by law, including merchantability or fitness for any particular purpose.

Please note that these rights do not automatically extend to content, data or other material published by Springer Nature that may be licensed from third parties.

If you would like to use or distribute our Springer Nature journal content to a wider audience or on a regular basis or in any other manner not expressly permitted by these Terms, please contact Springer Nature at

onlineservice@springernature.com